Chapter 11. Mechanical Behavior of Materials

11.1 Introduction

In service, materials are subjected to mechanical loads of various intensities, types and duration. The response of the material to these applied loads is termed *mechanical behavior*, and it is one of the most important factors in materials design. The most important questions to be answered are:

How and when does the material undergo permanent deformation?

When does the material fracture or otherwise fail?

These apparently simple questions are addressed in the field of mechanical behavior of materials. The answers depend on whether the load is applied quickly or over a period of time, whether the material is pulled in one or in more than one direction at once (uniaxial or multi-axial loading), whether the load is cyclic, and whether there are pre-existing flaws on the material. The ability of the material to resist deformation and failure under such conditions is measured by various mechanical properties, such as strength, ductility and toughness. These macroscopic material properties and their link to the underlying material microstructures are discussed in this chapter.

11.2. Mechanical Testing

Quantitative knowledge of material behavior comes from various mechanical tests from which material properties can be determined. To instruct the discussion, some mechanical tests and the mechanical properties they determine are described in the following.

11.2.1. Uniaxial Tensile Test

A specimen of uniform cross section (usually cylindrical) is uniaxially loaded and its deformation measured as a function of the applied load (Fig. 11.1).

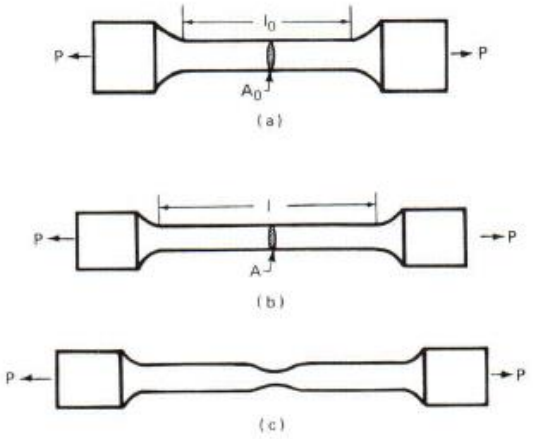

Fig. 1.1 Schematic of specimen deformation during a uniaxial tensile test.

A specimen of initial gauge length l_o and cross-sectional area A_o is subjected to an increasing tensile load P, applied along its axis and the resulting specimen deformation is measured. Upon application of the load the specimen gauge length increases to l and the cross-sectional area is reduced to A. The *engineering stress* is defined as:

$$\sigma_{eng} = \frac{P}{A_o} \tag{11.1}$$

but since during deformation the specimen cross sectional area is reduced from A_o to A, the *true stress* is

$$\sigma_{true} = \frac{P}{A} \tag{11.2}$$

Similarly, the *engineering strain e* is

$$e = \frac{l - l_o}{l_o} \tag{11.3}$$

while the *true strain* ε is the integral of the increments of strain along the specimen length:

$$\varepsilon = \int_{l_o}^{l} \frac{dl}{l} = \ln\left(\frac{l}{l_o}\right) \tag{11.4}$$

The true strain in tension is always somewhat larger than the engineering strain. For plastic deformation, volume is conserved:

$$Al = A_o l_o \tag{11.5}$$

From (11.5) and (11.4)

$$\varepsilon = \int_{A_o}^{A} \left(-\frac{dA}{A}\right) = \ln\left(\frac{A_o}{A}\right) \tag{11.6}$$

The strain in the loading direction implies a strain of $\varepsilon_t = \nu\varepsilon$ in the two transverse directions, where ν is Poisson's ratio[1]. If the material is isotropic, volume conservation implies $2\varepsilon_t + \varepsilon = 0$, which yields $\varepsilon_t = -0.5\varepsilon$.

The results of a tensile test are now examined. If the applied stress is plotted against the specimen strain we obtain the stress-strain curve, a schematic example of which is shown in Figure 11.2.

[1] Poisson's ratio is the ratio of the strain normal to the load to the strain along the load direction

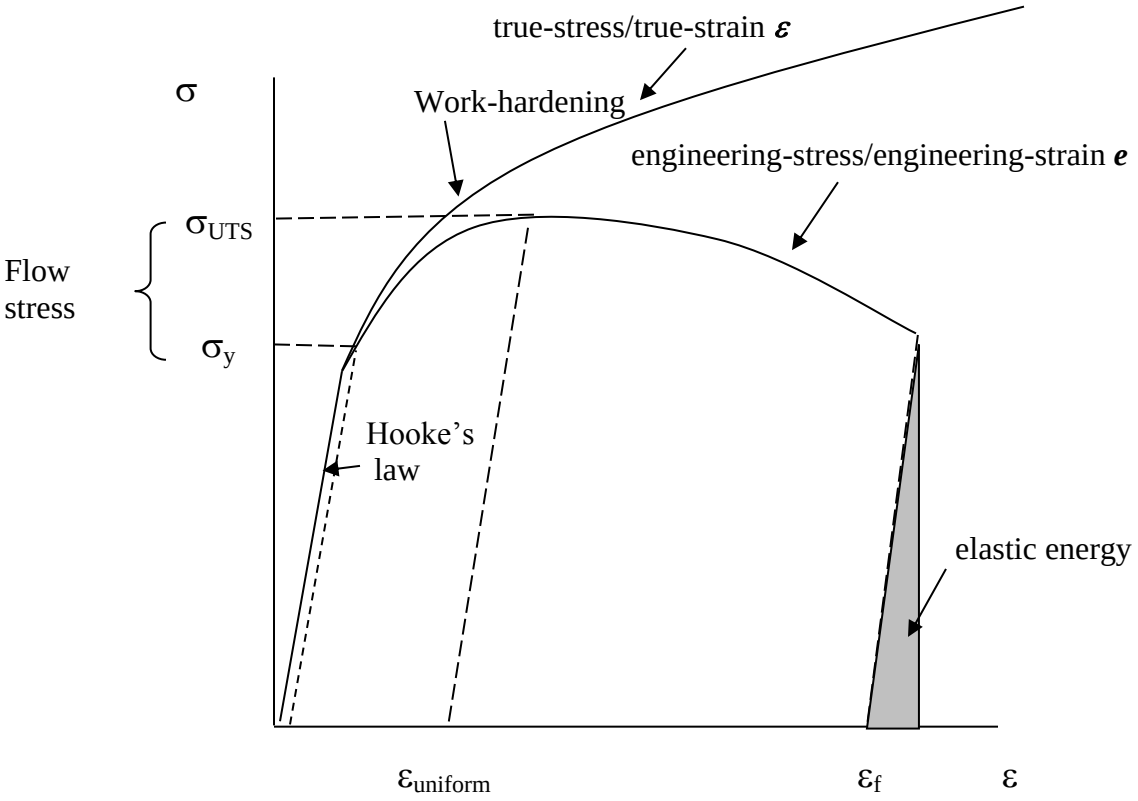

Fig. 11.2: Schematic stress-strain behavior typical of an austenitic steel.

From zero up to the yield stress, the material deforms elastically (i.e., reversibly) such that the strain is linearly proportional to the stress according to Hooke's Law:

$$\sigma = E\varepsilon \tag{11.7}$$

where *E* is Young's modulus or the elastic modulus. The region of validity of Hooke's law is the *elastic region*. This region is characterized by small *reversible* deformation: that is, once the load is removed, the strain disappears. In the elastic region, the engineering stress/engineering strain curve is coincident with the true stress/true strain curve. Typical values of Young's modulus and Poisson's ratio are shown in Table 11.1. Note that both Young's modulus and the yield stress decrease with temperature, as the material softens.

Material	**E (GPa)**	**ν (Poisson's ratio)**
Aluminum	70	0.35
Gold	78	0.44
Iron	211	0.29

Nickel	199	0.31
Tungsten	411	0.28
HT-9	160	0.33
Stainless Steel	190-205	0.26-0.29
Alloy 690	211	0.289
T91	206	0.33
Zirconium <1120>	99	0.37-0.40
Zirconium <0001>	125	

Table 11.1 Elastic moduli and Poisson's ratios of different materials at room temperature.

Above the yield stress material deformation starts to deviate from Hooke's law as a result of *plastic*, or irreversible, deformation. In order to establish a definite onset of plastic deformation, a minimum deviation from Hooke's law (normally 0.2%) is taken to be the point at which plastic deformation begins. The stress at which this occurs is called the *yield stress*, σ_y, beyond which the material deforms plastically, and is an important property of engineered materials. Note that some alloys, notably bcc materials, exhibit more complex yield behavior wherein the stress reaches an upper yield point before dropping down to a lower one [1].

The stress required for further deformation beyond the yield point may continue to increase because of *work hardening*, (also called *strain hardening*) often described by an equation of the form:

$$\sigma = K\varepsilon_p^n \tag{11.8}$$

where σ is the stress above σ_y, ε_p is the plastic strain, n is the *work-hardening exponent* and K is a constant, called the *strength coefficient*. Once yielding occurs the stress required to continue plastic deformation is called the *flow stress*. At the yield point the flow stress is equal to the yield stress, but it is higher than the yield stress in the work-hardening region (Fig. 11.2).

During tensile deformation the material deformation occurring in the elastic region and in the beginning of the work-hardening region is *uniform*, that is, all the material within the gauge section participates equally in the deformation process. At a strain corresponding to the ultimate tensile strength (σ_{UTS}) diffuse *necking* sets in, causing deformation to become non-uniform. A small variation in cross sectional area in the gauge section of the material can cause a slightly larger stress at that location, which causes larger deformation, in turn further diminishing the area.

As a consequence, once necking starts the specimen loses load carrying capacity, since the cross-sectional area (A) in the necked region becomes progressively smaller, and thus no additional load (P) is needed to cause further deformation. The stress at which necking

occurs is called the *ultimate tensile strength* of the material or σ_{UTS}. This is the maximum load-bearing capacity of the material. The strain at which necking occurs is the *uniform strain,* $\varepsilon_{uniform}$, and is one measure of the *ductility* of the material (i.e. how much can the material deform before failing). As deformation proceeds, the neck becomes progressively thinner until the material fractures. The *percent elongation to failure (%EL)* represents another measure of material ductility.

Another quantity that can be obtained from Figure 11.2 is the *toughness* of the material or the energy absorbed during fracture. This is the area under the curve minus the shaded region on the right, which represents the elastic energy stored in the material and which is recovered upon fracture. The more energy the material can absorb before fracturing, the higher its toughness.

11.2.2. Biaxial Testing: Tube Burst

The uniaxial tensile test described above is experimentally convenient and its theoretical interpretation is straightforward because only the normal stress σ_{xx} is active (stress in the direction of the rod axis). However, the stress in the nuclear fuel cladding and other core materials are often *biaxial* or *triaxial*. For example the stress- state of cladding subject to fission-gas pressure closely resembles that in a long thin-walled cylindrical tube closed at both ends and pressurized by a gas. This state of stress is biaxial, with components in the axial and hoop (azimuthal) directions.

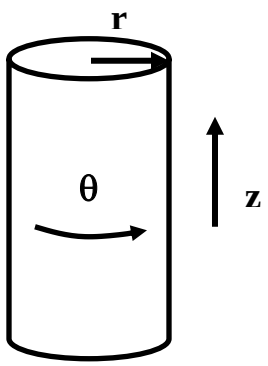

Figure 11.3: Geometry for a tube burst test

The response of tubing to biaxial stress is studied by a tube-burst test, for which (Sect. 6.5):

$$\sigma_\theta = \frac{pr}{\delta} \tag{11.9}$$

$$\sigma_z = \frac{pr}{2\delta} \tag{11.10}$$

$$\sigma_r \cong 0 \tag{11.11}$$

where *p* is the internal pressure, *R* is the tube mean radius and δ is the tube-wall thickness. For the tube to be considered thin walled the ration of wall thickness to tbe radius should be smaller than ***.

11.2.3. The Von Mises Equivalent Stress

In order to analyze plastic deformation and the yield condition in multiaxial stress configurations, the concept of an *equivalent stress* is employed. By definition, a uniaxially-loaded specimen yields when the stress reaches σ_y. Under multiaxial loading, a yield criterion was developed by von Mises [1]. This criterion is derived here for the case of the tube-burst test based on an equivalent stress.

Von Mises' general yield criterion is based on the difference between the total energy density under a multiaxial state of stress ($\mathcal{E}_{el}$) and the energy density resulting in the material when subjected to the mean of the three principal stresses, ($\bar{\mathcal{E}}_{el}$). When this difference reaches a critical value $\mathcal{E}_{el}^{*}$, i.e., when

$$\mathcal{E}_{el} - \bar{\mathcal{E}}_{el} > \mathcal{E}_{el}^{*} \tag{11.12}$$

the material will undergo plastic deformation. The mean of the three principal stresses is given by

$$\sigma_m = \frac{1}{3}(\sigma_1 + \sigma_2 + \sigma_3) \tag{11.13}$$

The elastic strain energy density $\mathcal{E}_{el}$ as a result of applied stresses is given by Eq (6.31):

$$\mathcal{E}_{el} = \frac{1}{2E}\left(\sigma_1^2 + \sigma_2^2 + \sigma_3^2\right) - \frac{\nu}{E}\left(\sigma_1\sigma_2 + \sigma_1\sigma_3 + \sigma_2\sigma_3\right) + \frac{1}{2G}\left(\sigma_{12}^2 + \sigma_{13}^2 + \sigma_{23}^2\right) \tag{11.14}$$

which for a solid under hydrostatic stress (no shear stresses) simplifies to

$$\mathcal{E}_{el} = \frac{1}{2E}\left(\sigma_1^2 + \sigma_2^2 + \sigma_3^2\right) - \frac{\nu}{E}\left(\sigma_1\sigma_2 + \sigma_1\sigma_3 + \sigma_2\sigma_3\right) \tag{11.15}$$

Substituting $\bar{\sigma}$ for σ_1, σ_2 and σ_3 in equation (11.15) yields the value of the homogeneous (average) elastic energy density

$$\bar{\mathcal{E}}_{el} = \frac{1-2\nu}{6E}(\sigma_1 + \sigma_2 + \sigma_3)^2 \tag{11.16}$$

Subtracting equation (11.16) from (11.15) we obtain

$$\mathcal{E}_{el} - \bar{\mathcal{E}}_{el} = \left(\frac{1+\nu}{6E}\right)\left[(\sigma_1-\sigma_2)^2 + (\sigma_2-\sigma_3)^2 + (\sigma_1-\sigma_3)^2\right] \qquad (11.17)$$

By setting equation (11.17) equal to the elastic energy density in the case where there is only one applied stress allows to obtain the critical equivalent stress σ_{eq} The elastic energy density difference for a uniaxial stress σ_{eq} that is "equivalent" to the 3-component hydrostatic stress is determined by setting $\sigma_1 = \sigma_{eq}$, $\sigma_2 = \sigma_3 = 0$ in eq. (11.15)

$$2\left(\frac{1+\nu}{6E}\right)\sigma_{eq}^2 = \left(\frac{1+\nu}{6E}\right)\left[(\sigma_1-\sigma_2)^2 + (\sigma_2-\sigma_3)^2 + (\sigma_1-\sigma_3)^2\right] \qquad (11.18)$$

from which we obtain the von Mises equivalent stress

$$\sigma_{eq} = \frac{1}{\sqrt{2}}\left[(\sigma_1-\sigma_2)^2 + (\sigma_2-\sigma_3)^2 + (\sigma_1-\sigma_3)^2\right]^{1/2} \qquad (11.19)$$

Eq. (11.19) is an important and widely used relation that predicts the onset of plastic deformation (yielding) in an engineering component subjected to multiaxial stresses.

The equivalent stress for the uniaxial tension case can be computed by noting that $\sigma_1 = \sigma_x; \sigma_2 = \sigma_y = 0$ and $\sigma_3 = \sigma_z = 0$, which yields $\sigma_{eq} = \sigma_x$. Note that at the yield stress $\sigma_{eq} = \sigma_y$; again showing that Eq. (11.19) can predict yielding in multiaxial stress states if the yield stress is known.

For the tube burst case, substituting equations (11.9) to (11.11) into yields

$$\sigma_{eq} = \frac{\sqrt{3}}{2}\sigma_\theta \qquad (11.20)$$

This equation permits plastic properties determined by the uniaxial tensile test (Sect. 11.2.1) to be applied to the response of a pressurized tube. For example, if the yield stress measured in the uniaxial test is σ_y, a pressurized tube should yield at a hoop stress of

$$(\sigma_\theta)_{yield} = \frac{2}{\sqrt{3}}\sigma_y \quad \text{or a pressure of} \quad p_{yield} = \frac{2}{\sqrt{3}}\frac{\delta}{R}\sigma_y \qquad (11.21)$$

Since the equivalent stress derived above defines yielding in a multiaxial stress state, Eq (11.19) defines a *yield locus*, which is a surface in three-dimensional space. The yield locus for two-dimensional *plane stress* ($\sigma_3 = 0$) is analyzed in Example # 1.

Example #1 Yield locus for plane stress

To determine the locus of points at which a specimen yields, Eq (11.19) for plane stress with $\sigma_{eq} = \sigma_y$ is written as:

$$\sqrt{2} = \left[(x-y)^2 + x^2 + y^2 \right]^{1/2} \tag{11.22}$$

where :

$$x = \frac{\sigma_1}{\sigma_y} \qquad \text{y} = \frac{\sigma_2}{\sigma_y} \tag{11.23}$$

Solving Eq (11.22) for y:

$$y = \tfrac{1}{2}\left[x \pm \sqrt{4 - 3x^2} \right] \tag{11.24}$$

Equation (11.24) is plotted in Fig. 11.4.

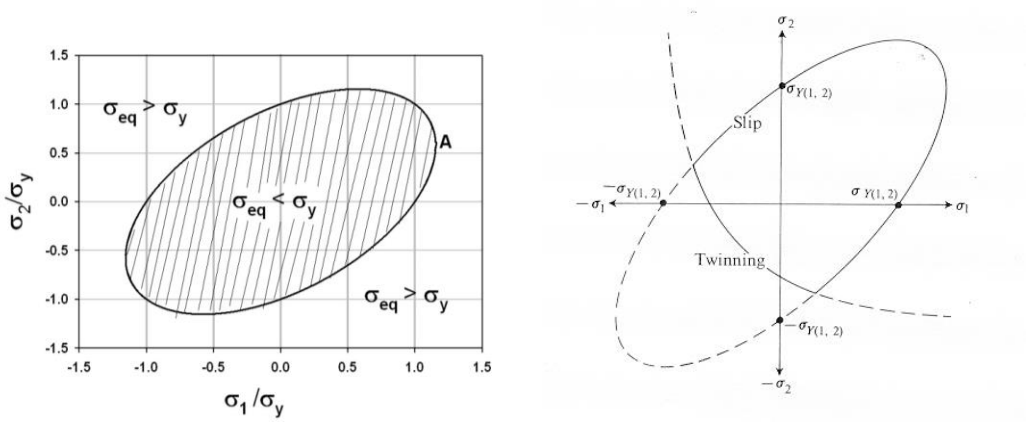

Fig. 11.4 (left) Yield locus for plane stress . (right) Yield Loci for slip and twinning in a hexagonal close-packed sheet, after [2]

For any and all combinations of the two stress components σ_1 and σ_2 which fall inside the tilted ellipse, the specimen does not yield, such that the material behaves elastically (described in Chapter 6). All conditions outside the oval cause the specimen to yield.

The yield locus shown on the left in Fig.11.4 is *symmetric* with respect to the deformation direction, i.e. it is the same in tension or compression as well as along the two orthogonal in-plane directions (e.g., x-y, θ-z). This has an important implication, valid for most metals, that the yield stress in tension is the same as in compression as long as there is no change in deformation mechanism.

Example #2 Application of Plane stress yield locus to a pressurized tube
Let $\sigma_1 = \sigma_\theta$ and $\sigma_2 = \sigma_z$; for the pressurized tube, Eqs (11.9) and (11.10)

are $\sigma_1 = 2\sigma_2$
or, in terms of Eq (11.23), $y = \frac{1}{2}x$. When this relation is substituted into Eq (11.22), the solution is $x^2 = 4/3$ or $x = 2/\sqrt{3}$, which is the same as Eq (11.21)
To locate this point on Fig. 11.4, $x = 2/\sqrt{3} = 1.155$ and $y = 1/\sqrt{3} = 0.577$. This is point A on Fig. 11.4.

The yield locus shown on the left in Fig.11.4 is symmetric with respect to the deformation direction, i.e. it is the same in tension or compression as well as along the two orthogonal in-plane directions. However, not all materials deform isotropically– zirconium, for example, has different yield stresses along different deformation directions. Figure 11.4 (right) shows the yield locus for textured hcp sheet material. The locus is more elongated than that in Fig. 11.4 (left) which means it does not obey Eq.(11.22).

The yield locus depends on the mechanisms of deformation, which could reduce the yield locus (i.e. achieve plastic deformation at a lower stress than the von Mises criterion). For example, figure 11.4 right also shows a line that under compressive stress, twinning is favored over slip as it occurs at lower strains.

11.2.4. Hardness Testing

Hardness testing is a comparatively easy way to obtain information about the deformation behavior of a material. In this test, an indenter –typically in the form of a ball or a pyramid – is applied with a certain force to a material. The indenter is much harder than the material tested, so that to a good approximation only the latter deforms plastically. For a given force, the indenter penetrates a certain depth into the material, which is measured microscopically by the area of indentation.

As the indenter penetrates, the material flows plastically under it. . The stress required for such deformation to occur is the *flow stress* (see text after equation (11.8). The elastic region near the indent constrains the deformation so that a much larger stress than the yield stress is needed to cause plastic flow. For a spherical indenter the relationship from which σ_y can be estimated is [3]:

$$p = \frac{4P}{\pi d^2} \cong a\sigma_y \qquad (11.25)$$

where a = 2.5 – 3.0 depending on the material, and where p is the pressure on the indenter needed for penetration, P is the applied load and d is the diameter of the indentation.

There are several types of hardness tests, depending on , indenter shape and measurement of indent area or depth. Typical examples include Brinell, Meyer, Vickers and Rockwell tests. It is also possible to perform hardness testing on a microscale by using an indenter that is smaller than the dimension of one grain.

11.2.5. Impact Testing

Impact tests can be used to measure the fracture resistance of the material. Fracture energy is the area under the stress-strain curve up to fracture (Fig. 11.2) It is a measure of the ability of the material to deform plastically before fracture in the *absence* of a pre-existing crack. However, for failure analysis of nuclear components, it is often required to assume the *presence* of a crack, and show that it does not propagate. The resistance of the material to crack propagation is given by the *fracture toughness* of the material, rigorously measured using specially designed specimens into which a fatigue pre crack is induced. However the impact test energy can be empirically related to the fracture toughness, as exemplified below.

The Charpy impact test is commonly used in the nuclear industry, for example, for assessing the degree of embrittlement suffered by the pressure vessel after exposure to neutron irradiation. In the Charpy test a large hammer swung from a pendulum is released from an initial height h_1 towards a specimen into which a v-notch groove has been machined (Fig. 11.5). The high speed of the hammer and the presence of the notch cause the material to be deformed at a high strain rate and in a triaxial state of stress, both of which favor fracture. The kinetic energy of the hammer is sufficient to break the sample. Subsequent to specimen fracture the hammer continues along its arc, rising to a height $h_2 < h_1$. The energy absorbed by the specimen during fracture is given by:

$$E_{abs} = mg(h_1 - h_2) \tag{11.26}$$

where m is the mass of the hammer and g is the gravitational constant. A brittle material (such as glass) absorbs little energy as it breaks, while a ductile sample absorbs more energy before fracturing. The test is repeated at several temperatures and E_{abs} is plotted vs. temperature. For some materials, in particular ferritic steels, the energy absorbed shows an abrupt change at a temperature called the *ductile-to-brittle transition temperature* (DBTT).

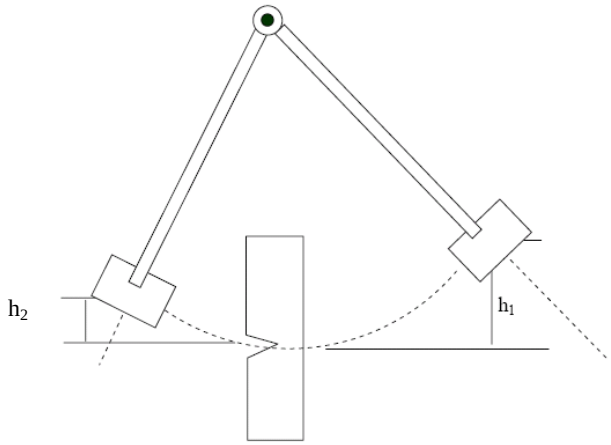

Figure 11.5. Schematic geometry of a Charpy v-notch impact test. (note that in an actual Charpy test the specimen would be positioned horizontally; it is shown vertically for clarity)

Figure 11.6, shows schematically the energy absorbed during a Charpy impact test as a function of test temperature. For materials showing the ductile to brittle transition, the absorbed energy is high at elevated temperature, undergoes a decrease within a relatively narrow interval as the temperature is decreased, then remains low thereafter. The energies absorbed at high and low temperature are called the *upper-shelf energy* and *lower-shelf energy*, respectively. The midpoint of the transition from the upper-shelf to the lower-shelf energy (the Charpy V-notch energy, or CVN) occurs at the *ductile- to-brittle transition temperature* (DBTT). For pressure-vessel steels the absorbed energy at the transition is 41 J.

The analyses of the fracture surfaces from testing at low and high temperatures reveal differences in fracture morphology. At low temperature the fracture surface is flat and shiny, indicating brittle failure by cleavage, while at high temperature a fraction of the cross-sectional area (the fracture surface) is dull, indicating partial ductile fracture. The degree of ductile failure can be quantitatively evaluated by the fraction of cross-sectional area that shows a ductile appearance. For low-to-moderate strength steels, the Charpy test is a good indicator of the material's fracture toughness. In fact the fracture toughness often exhibits a marked decrease in a similar temperature interval as does the absorbed energy [3].

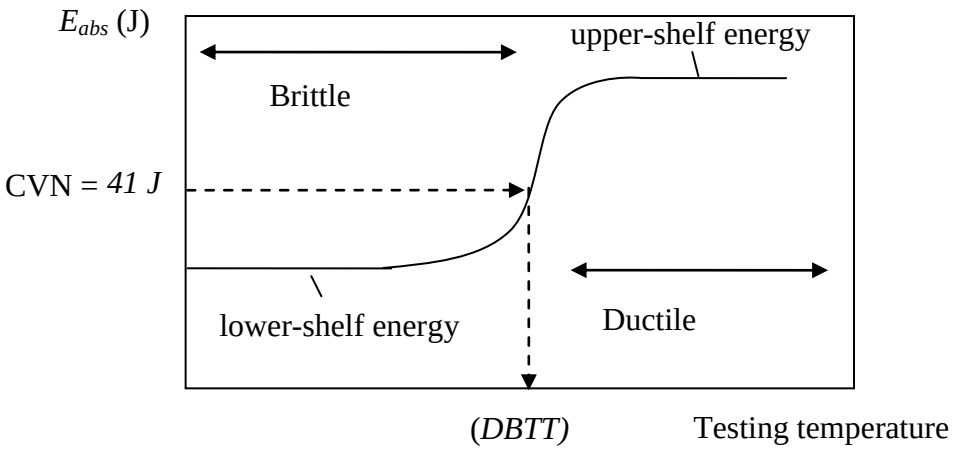

Fig. 11.6 Schematic representation of energy absorbed during a Charpy test as a function of testing temperature.

Empirical relationships can be obtained between the Charpy V-notch energy and the fracture toughness (K_{IC}, Sect.11.5.3) [4]. One such relationship is:

$$\left(\frac{K_{IC}}{\sigma_y}\right)^2 = \frac{5}{\sigma_y}\left(CVN - \frac{\sigma_y}{20}\right) \tag{11.27}$$

11.3 Microstructural Aspects of Deformation

Having reviewed some of the tests used to determine mechanical behavior we now turn to the underlying microstructural processes responsible for such behavior.

11.3.1. Critical Resolved Shear Stress and the Yield Stress

As discussed in Chap. 7, plastic deformation in real crystals is principally effected by the movement of dislocations, which requires the activation of multiple slip systems (combination of dislocations and slip planes). As discussed in Sect. 7.3 this occurs when the resolved shear stress exceeds the critical value for slip. For a single crystal the onset of slip coincides with the yield point.

However, real materials are polycrystalline and contain grains of different orientations with different susceptibilities for slip. As a result, a uniaxial applied stress deforms some grains more than others during the deformation process. Because the deformation of a given crystallite (grain) is constrained by neighboring grains, grain-to-grain incompatibilities arise which need to be accommodated by further plastic deformation.

A simple two-dimensional illustration of this concept is shown in Fig. 11.7. Consider two neighboring grains (a), which are oriented differently with respect to the loading axis (arrows) so that they shear in different directions.

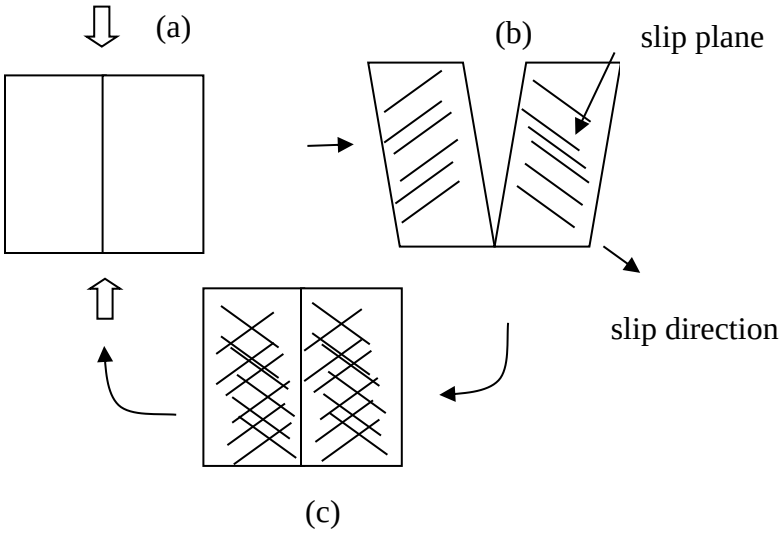

Fig. 11.7. Schematic of role of various slip systems in ensuring deformation compatibility (a) initial; (b) grain separation in the absence of grain-boundary adhesion (c) excitation of compensating slip systems to prevent grain-boundary separation

In such a thought experiment if the grains were free, the slip system in the left-hand grain deforms the grain to the left, while a different orientation of the same slip system in the grain on the right causes deformation in a different direction (b). In order to maintain the grain boundary intact, which is always the case in ductile materials, another slip system in the other direction is needed, (c), so that the deformation in both grains is nil, thus keeping the grains together.

In the case of a three-dimensional solid, the above process is repeated in three orthogonal directions, which means that *six* independent slip systems are needed for grain-to-grain compatibility during plastic deformation. However, the requirement of constant volume means one of the slip systems is not independent so that only *five* independent slip systems are needed to permit deformation in a polycrystalline solid.

For a given direction of the load P = Aσ, the resolved shear stress σ_{RSS} acting in a particular slip direction inclined by an angle λ with respect to the loading axis and contained in a plane with a normal inclined by ϕ from the loading axis is (see Eq (7.1)):

$$\frac{P}{A}\cos\lambda\cos\phi = \sigma_{\mathrm{RSS}} = \frac{\sigma}{m} \tag{11.28}$$

where the factor $1/m = \cos\lambda\cos\phi$ is the *Schmid factor* for the slip system, and *m* is a constant, sometimes known as the Taylor factor. When σ_{RSS} is large enough to activate

the slip system, it is equal to the *critical resolved shear stress* σ_{CRSS} for that slip system (Sect 7.3.1).

In a single crystal the equation

$$\sigma_y = m\sigma_{CRSS} \tag{11.29}$$

describes the yield condition. Note that while σ_y is the axial stress at yielding, σ_{CRSS} is the critical shear stress acting on the slip plane and in the slip direction (which by necessity lies on the slip plane).

In a polycrystal each of the five independent slip systems need to be operational to account for deformation incompatibilities (i.e., the angles of slip planes between adjacent grains, as in Fig. 11.7). For a given applied stress σ each slip system has a different Schmid factor and consequently a different critical resolved shear stress. For all five independent slip systems to be operative, the product of the applied normal stress σ and the Schmid factor needs to be higher than the critical resolved shear stress. Only under this condition can plastic deformation begin; this is the yield stress, σ_y.

Because several grains are involved in insuring deformation compatibility, it is not possible to directly relate Schmid factors and yield stress. The Schmid factor that activates a particular slip system depends on many factors, including the availability of slip systems, the ease of switching from one slip system to another, the texture of the material and the availability of other deformation mechanisms such as twinning (see Chap 17. However, a Schmid factor calculated by averaging the individual Schmid factors of the slip systems has been found to describe yield in polycrystalline materials Simulations conducted in both fcc and bcc materials show that the Taylor factor is 3.0-3.1 [5].

11.3.2. Strengthening Mechanisms

Several mechanisms exist for increasing the yield strength of a given material, all of which involve changing the microstructure so as to hinder dislocation motion by creating obstacles that dislocations must bend around or cut through, or altering the dislocation to a shape that impedes its motion. .

As shown in Eq (7.36), the critical stress to induce motion of dislocations through a field of hard obstacles by a looping process is the Orowan Stress

$$\sigma_c = \alpha \frac{2Gb}{\bar{l}} \tag{11.30}$$

where G is the shear modulus, b the burgers vector, and $\bar{l}$ is the mean spacing between the obstacles. Depending on the degree of uniformity of the obstacle array, $0.8 < \alpha < 1.0$, For a uniformly-distributed array of obstacles, $\alpha = 1$ [6].

The various hardening mechanisms refer to the various ways in which obstacles can be introduced into the material, as listed below.

- **Increase in dislocation density**: Once yielding starts, dislocation tangling generates mobile dislocations by processes analogous to the Frank-Read sources (Sect. 7.11.2). A large fraction of these dislocations become entangled and sessile, thereby creating a long-range internal stress field which hinders the motion of the mobile dislocations, causing the stress required for further deformation to increase according to Eq (7.36). This is one of the principal causes of the work-hardening behavior discussed in Sect 11.2.1. Like work-hardening (Fig. 11.2), *cold- working* increases the density of tangled and *sessile* (immovable) dislocations.

- **Grain boundary strengthening**: A similar hindrance to the motion of mobile dislocations is caused by *grain refinement*. As the grain size becomes smaller, the distance between grain boundaries decreases, and since these also impede dislocation motion, the stress required for deformation correspondingly increases.

- **Solid Solution hardening**; this is due to the addition of foreign atoms, either in solid solution. In solid- solution hardening, dislocations are pinned to impurities in the crystal. If the impurity atom size is substantially different from that of the matrix atoms, the strain-energy interaction between the solute atoms and the dislocation "anchors" the latter.

- **Particle hardening**: In precipitation *hardening* the insoluble impurity elements precipitate and these precipitate particles become obstacles to dislocations glide. Dislocations either cut through small precipitate particles or bend around large particles and hardening is approximated by Eq (11.30). Thus, a high density of small particles with small spacing results in high strength. In either case, the critical resolved shear stress is increased.

A review of strengthening mechanisms is available in references [5, 6].

11.4. Creep Deformation

The tests described in Sect. 11.2 determine the *instantaneous* material response, that is, the response obtained when the structure of the material does not appreciably change during the test, as is the case at temperatures less than one third of the melting temperature. At higher temperature, diffusion of atoms results in time-dependent deformation (*creep)* that occurs if the load is applied over a long period of time. One simple example is the deformation of a spring. If the spring is stretched in the elastic regime ($\sigma<\sigma_y$) and quickly unloaded, it returns to its original shape. However if the load is applied over a long period strain may not be recovered upon unloading, i.e., the spring has plastically deformed. This slow (time-dependent) plastic deformation at a stress lower than the yield stress is called *creep*.

Whether creep resistance or mechanical strength limits performance depends on the temperature/stress combination [7]. At fixed temperature, when the applied stress is smaller than that required for yielding, slow-strain-rate deformation can occur by creep. Similarly, for a fixed stress, yielding occurs at high temperature, while creep is restricted to lower temperatures.

11.4.1. Phenomenological Description of Creep

Creep under a constant load can be divided into the three stages shown in Fig. 11.9.

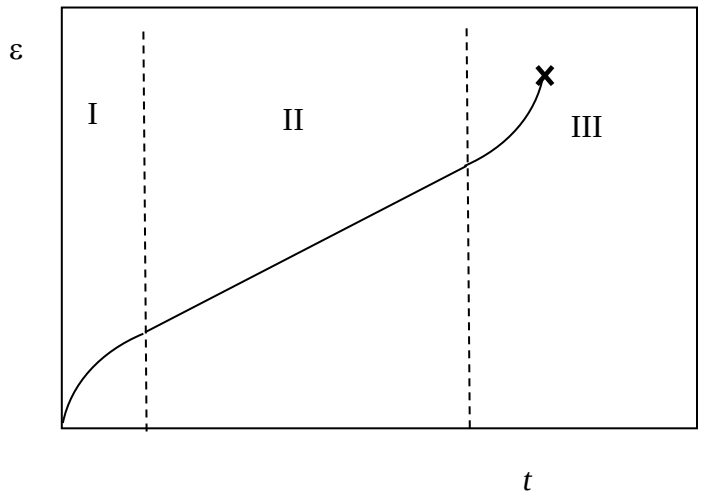

Figure 11.9: Schematic description of creep strain versus time at fixed temperature. The X indicates fracture

- Stage I: The initially-high strain rate decreases with deformation (or time). This stage is akin to strain-hardening (Fig. 11.2) in which creep deformation changes the material structure and the strain rate $(d\varepsilon/dt)$ decreases with time and strain.

- Stage II:When thermal deformation recovery and deformation hardening match, *secondary creep*, which is characterized by a constant strain rate, begins. This stage may last the greater part of the material lifetime.

- Stage III: or *tertiary creep;* the strain rate increases and rapidly leads to failure (X in Fig. 11.9))

11.4.2 Creep lifetime

Creep life is usually dominated by stage II, for which the steady-state strain rate is described empirically by the Dorn equation, which is a power law equation of the form:

$$\dot{\varepsilon}_{II} = A\sigma^n \exp\left(-\frac{Q}{k_B T}\right) \tag{11.31}$$

where A and n are material constants, σ is the applied stress and Q is the activation energy for creep. For small grain sizes, A may be a function of grain size, especially at high temperatures, where grain boundary sliding becomes more prevalent. Often stage II dominates the time to failure and the strain at fracture is given by

$$\varepsilon_f = \dot{\varepsilon}_{II} t_f \tag{11.32}$$

where t_f is the creep life of the material.

11.4.3 Larson-Miller Plots

Larson-Miller plots are a convenient method of predicting and comparing the creep strengths of engineering alloys. Taking the logarithm of both sides in Eq (11.31) we obtain:

$$\ln \dot{\varepsilon}_{II} = -\frac{Q}{k_B T} + ln(A\sigma^n) \tag{11.33}$$

If stage II dominates then inserting Eq (11.32) into the above yields:

$$\ln(A\sigma^n) - \ln\left(\frac{\varepsilon_f}{t_f}\right) = \frac{Q}{k_B T} \tag{11.34}$$

From Eq (11.34) we define the Larson-Miller parameter LM by:

$$T[\ln t_f + C] = \frac{Q}{k_B} = LM \tag{11.35}$$

Here Q/k_B = LM (units of Kelvins) is a material constant and the terms on the left hand side of the equation are the parameters of the creep test (temperature and time-to-failure). The LM parameter is a good indicator of a material's creep resistance. Figure 11.10 shows LM plots for various steels. [8, 9]. In this case Eq(11.35) is slightly modified to

$$T(\ln t + 30)\times 10^{-3} = LM \tag{11.36}$$

Note that Eq. (11.36) is only approximately satisfied (a straight line would be expected to result if it did).

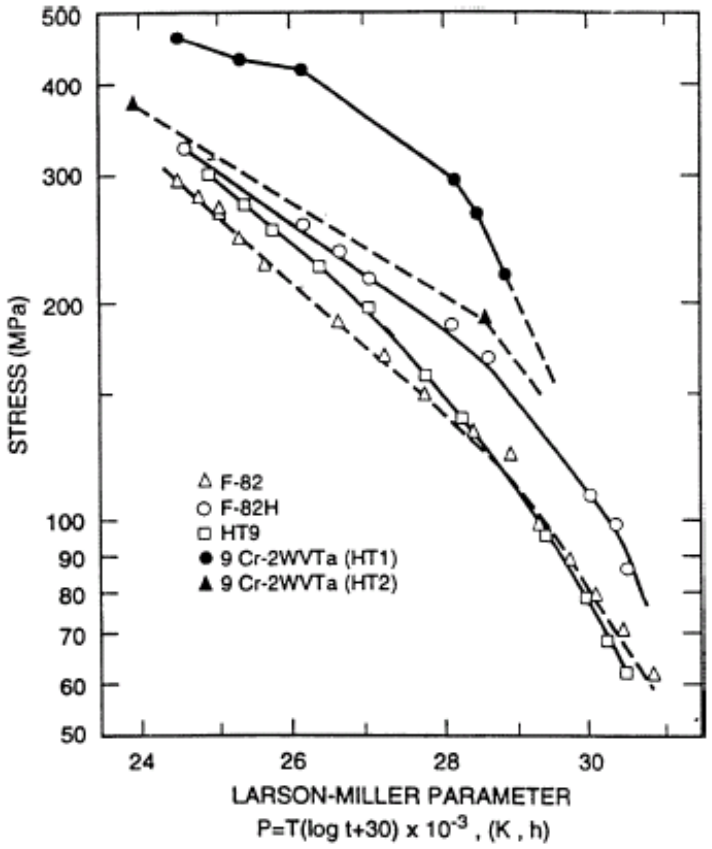

Figure 11.10: Larson-Miller plots for various ferritic-martensitic steels considered for advanced reactors.[9]

Example #3: Use the LM plot to determine the maximum allowable stress for HT-9 when operated at 700 K, so that failure does not occur before 24x365 h (~ 1 year).

The LM parameter under these conditions is LM=700(ln(8760)+30)x10^{-3}= 27.4 so that the maximum allowed stress is ~140 MPa.

Conversely it is also possible to estimate the creep life under a given applied stress and temperature. For example for a stress of 100 MPa at 700 K alloy F-82 shows a LM parameter of 29 which translates to a creep life of 10.5 years. At 200 MPa for the same conditions the LM is approximately 26 and the creep life would be about 52 days.

11.4.4. Creep Mechanisms

Contrary to low temperature deformation, creep is thermally-activated relying on several mechanisms, such as dislocation climb and glide or diffusional flow of atoms and point defects. These mechanisms are briefly reviewed here.

Thermally-enhanced glide
Computer simulations have shown that a dislocation in a crystal is constantly "vibrating", or changing shape because of the motion of atoms of which it consists. . As the critical shear stress is approached, atom thermal motion provides the additional push that allows it to glide. This mechanism is also active at low temperature, so it is not limited to creep deformation.

Thermally-induced dislocation glide (climb - glide)
An edge dislocation can be stopped in its slip plane by an obstacle which exerts a back force greater than the forward force from the applied stress. Glide can continue on an alternate slip plane by diffusional absorption of one type of point defect. This allows the dislocation to *climb* to another plane where the retarding force exerted by the obstacle is smaller and can be overcome by the forward force, thus permitting glide to continue.

Figure 11.11 illustrates this mechanism.

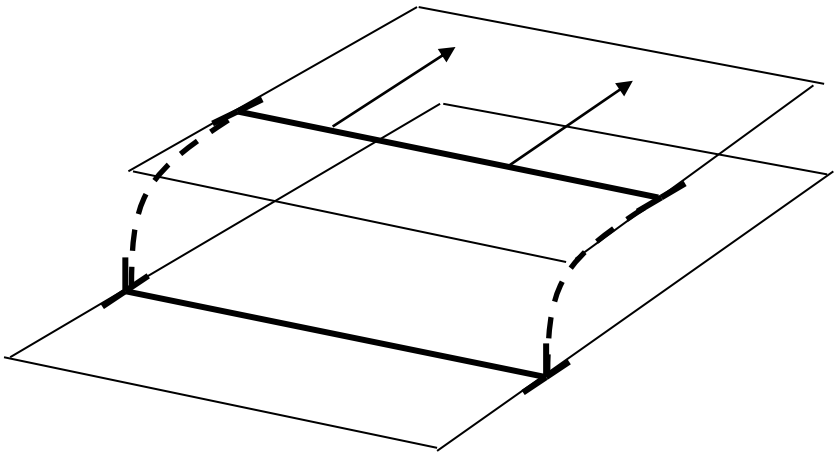

Fig. 11.11 Thermally-enhanced climb-and-glide creep

ThermallyAcivated Recovery

As material deforms, dislocations multiply, most becoming entangled and sessile, forming long range stresses which serve as barriers to dislocation motion. At elevated temperatures, a dislocation climb process enables such entagled dislocations to reorganize into lower energy configurations. This recovery process decreases the back stress to mobile dislocations permitting glide and consequent deformation to continue.

Stress Induced Diffusional Flow Difference (Nabarro-Herring Creep)
When a stress is applied, the equilibrium concentration of vacancies in the solid adjacent to the grain boundaries is altered (see Chap. 4). Tensile stress augments the vacancy concentration relative to that in the unstressed solid and a compressive stress reduces it. In the left-hand diagrams in Fig. 11.12, there is no tensile stress on the vertical grain boundaries due to the applied stress indicated, so the vacancy concentration in adjacent solid is not affected. On the tilted boundaries, however, there is a component of tensile stress, hence the nearby vacancy concentration is increased. Therefore a flux of atoms as shown by the arrows and the grain deforms in the direction of the applied load.

Coble Creep
In the same manner as in Nabarro-Herring creep, Coble creep occurs because of a vacancy gradient induced by the mechanical loading of the specimen. However mass transport takes place in the grain boundaries rather than in the lattice adjacent to them. This mechanism also causes an overall grain extension and deformation in the direction of loading.

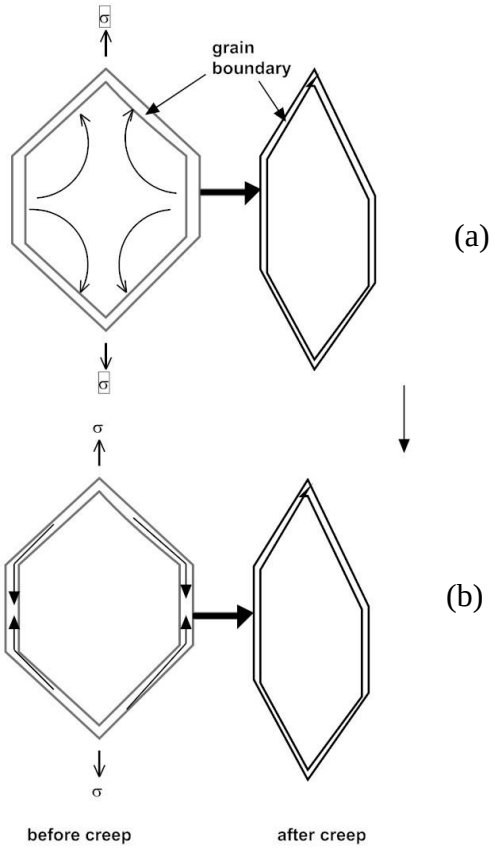

Fig. 11.12 (a) Nabarro-Herring and (b) Coble Creep

Thermally Induced Grain Boundary Sliding
At high temperatures, grain boundaries inclined to the stress can slide providing that vacancies can diffuse and move material to accommodate grain- grain incompatibilities (Fig. 11.7) that would otherwise occur. The process obeys equation (11.31), where the constant A increases with decreasing grain size.

11.4.5. Deformation Mechanism Maps

Ashby and co-workers [10] have displayed the various deformation mechanisms on a single map (Fig. 11.13) In the region $\sigma > \sigma_y$, plastic deformation occurs by general yielding, which corresponds to dislocation glide. At higher stresses the theoretical shear strength of the material is reached. At $\sigma < \sigma_y$ plasticity can occur by several creep mechanisms, each activated at different temperatures.

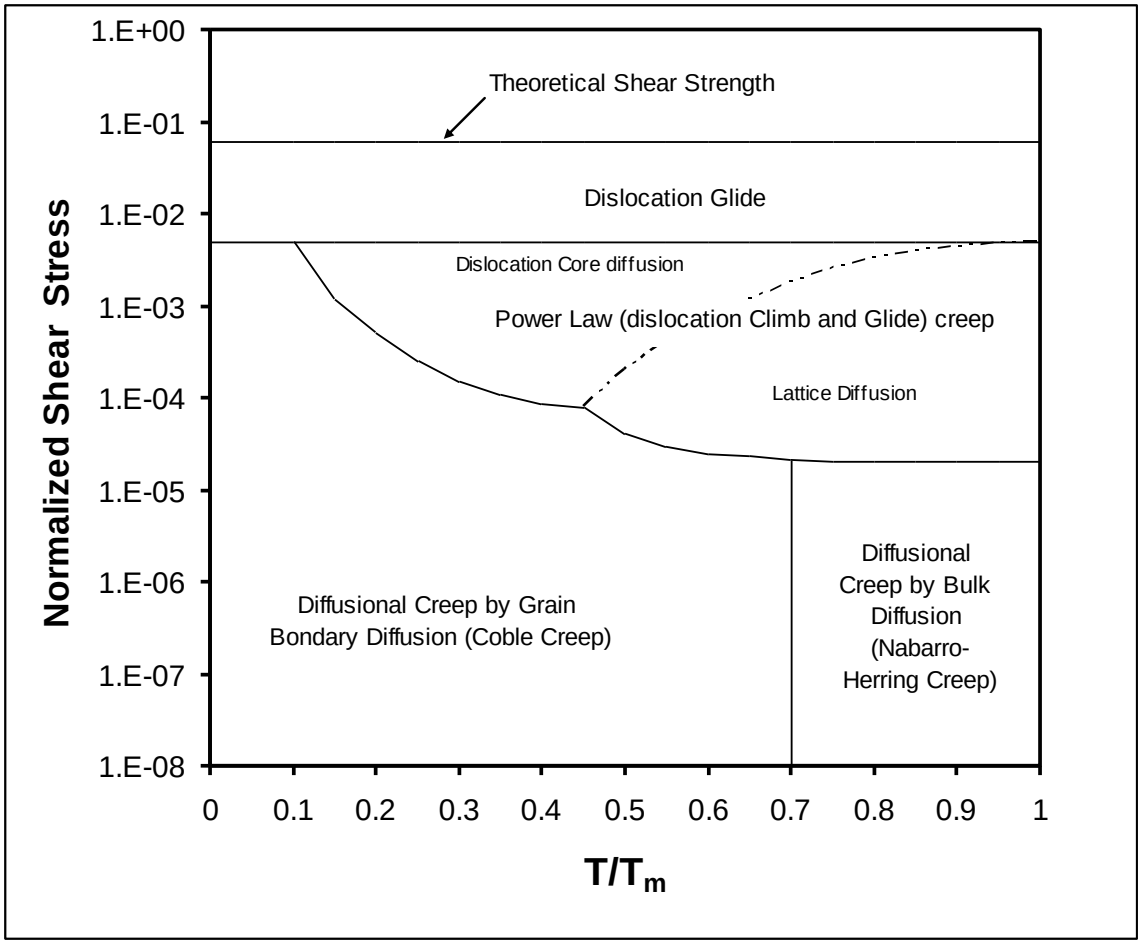

Figure 11.13: Schematic creep deformation mechanism map for pure nickel with a grain size of 1 μm [10]. Grain boundary sliding is insignificant. The stress is normalized to the shear modulus (σ/G) and the temperature to the melting temperature.

Creep under irradiation is discussed in Chap 27.

11.5. Material Fracture

Increasing material deformation eventually leads to fracture, which is discussed briefly in this section. Most fractures of structural metals occur due to one or more of the following processes:

• **Overload fracture** in which plastic deformation develops throughout the load-bearing cross section of the engineering component. Eventually, the plastic deformation drives a damage accumulation process within the metal, forming voids which subsequently grow and link as further plastic deformation occurs. The result is ductile fracture at stresses that exceed the yield stress. The component fractured through this process shows evidence of gross plastic deformation usually in the form of "necking" of the cross section at the fracture surface.

• **Failure due to crack growth** can occur when a crack is present and the external stress is sufficient to cause the crack-tip stress intensity to become critical at the *fracture toughness* of the material. Once the fracture toughness is exceeded, in most cases the crack propagates in an unstable manner causing abrupt fracture. Importantly, the applied stress is less than the yield stress of the material in such failures. The mechanism of crack growth may involve either ductile fracture or brittle fracture, but: (i) is confined to the crack-tip zone,(ii) occurs under elevated local tensile stresses, and (iii) often takes place at high deformation rates within a small crack-tip plastic zone. The result is fracture that looks brittle to the naked eye.
• **Failure due to *subcritical* crack growth** may occur when an existing small crack slowly propagates at a stress intensity smaller than the fracture toughness, as result of external factors such as, stress-corrosion cracking, hydrogen-assisted cracking or possibly load cycling (metal fatigue failure). Both stress-corrosion cracking and hydrogen assisted cracking are often intergranular resulting from grain boundary decohesion, as the grain boundaries can provide weak spots for crack growth. Up to 90% of all in-service failures occur slow, sub-critical stable crack growth until the crack reaches a length when it becomes critical at the fracture toughness of the material. Since the applied load is less than that of the yield stress, these time-dependent, "brittle-like" failures are almost always unexpected and can cause serious problems.

The three failure mechanisms are briefly reviewed in the following.

11.5.1. Overload Failure by Diffuse Necking: The Considère Criterion

As the material starts to deform plastically under tensile load, the strain is uniform (see Fig. 11.2), until the UTS where diffuse necking starts. Once a small deviation from uniform strain appears in the rod, such as shown in Fig 11.1(c), load-carrying capacity is lost; additional strain decreases the neck diameter causing the stress in the necked section to increase, which causes further deformation and so on. However, with deformation comes work hardening according to Eq (11.8), which raises the stress required to maintain plastic deformation. The onset of diffuse necking occurs when the material deforms faster than it can strain-harden is identified with the Considère criterion [11]

Necking initiates near the maximum load:

$$P = \sigma.A \Rightarrow dP = Ad\sigma + \sigma dA \tag{11.37}$$

and so when dP = 0,

$$\frac{dA}{A} = -\frac{d\sigma}{\sigma} = -d\varepsilon \therefore \frac{d\sigma}{d\varepsilon} = \sigma \tag{11.38}$$

Consider further that when a rod such as in Figure 11.1, subjected to a load P, initial length *l* and initial cross sectional area *A*, the material is deformed plastically to a length *l+dl* which results in a diminution of the cross-sectional area to *A'*. This causes the material to strain harden. If the material deforms according to Eq (11.8),

$$\sigma = K\varepsilon^n$$

The strain here is understood to be *plastic* strain. The change in strain hardening (dσ) caused by incremental strain $d\varepsilon$ *is:*

$$\frac{d\sigma}{d\varepsilon} = Kn\varepsilon^{n-1} = \frac{n\sigma}{\varepsilon} \tag{11.39}$$

Eqs (11.39) and (11.38) give the following criterion for plastic instability due to necking:

$$\varepsilon_U = n \tag{11.40}$$

where ε_U is the uniform true strain at the onset of necking (from Fig. 11.2). This equation, the Considère criterion [11], states that the strain at the onset of a necking instability the strain is numerically equal to the strain-hardening exponent *n*. For an engineering component loaded in uniaxial tension, the uniform strain also identifies the maximum load that components can sustain before failure occurs.

11.5.2. Ductile Fracture

Once necking starts, fracture occurs by damage accumulation. Due to the presence of hard second-phase particles or inclusions (e.g., intermetallic precipitates, carbides, sulfides or hydrides), deformation incompatibilities develop within the material as it plastically deforms. At small plastic strains these deformation incompatibilities are accounted for by other slip systems that allow particle-to-matrix interfaces to remain intact (Sect. 11.3.1). As deformation accommodation by activation of multiple slip systems becomes increasingly difficult, dislocation pileups and interactions, and h damage (such as voids or pores) accumulates near second-phase particles, interfaces and triple points. As shown schematically in Fig. 11.14 (b), larger strains nucleate voids at the particle-matrix interfaces or they may cause the particles to crack creating internal voids.

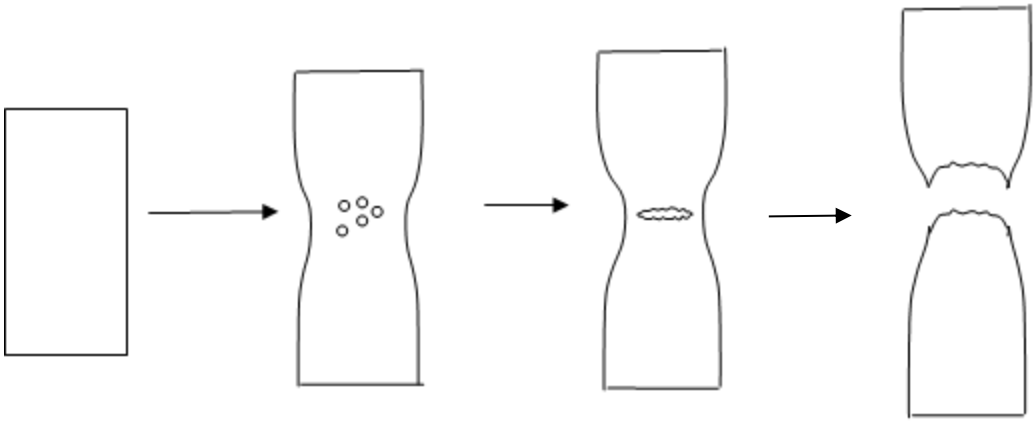

(a) (b) (c) (d)

Figure 11.11 Schematic representation of void formation and coalescence in ductile fracture.

Upon further straining of the rod, the voids grow and eventually coalesce as in Fig. 11.14(c). To predict failure (Fig. 11.14(d)), a void initiation criterion, a void growth law and a void coalescence condition are needed. Many such models have been developed [12] but are beyond the scope of this book.

As a result of the formation of voids before fracture (b) and their coalescence (c), the fracture surface will normally exhibit ductile dimples, as shown in Fig.11.15.

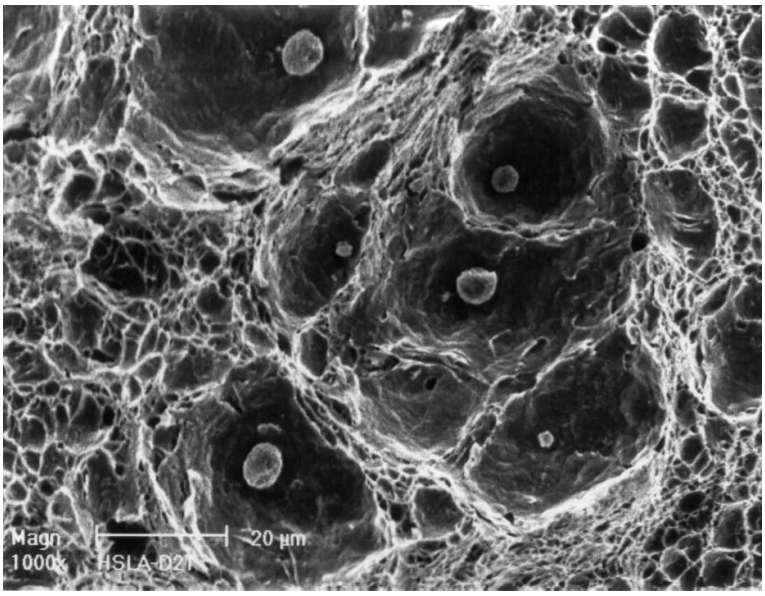

Fig.11.15 Micrograph showing the fracture surface of a steel containing spherical inclusions that initiate "primary" voids which are linked by small secondary voids during the ductile fracture process[13]

.

11.5.3. Fracture due to Crack Growth

The presence of a crack and its propagation and can cause early deformation and fracture (at stresses below the yield stress), representing an alternate path to failure. The analysis of crack propagation is reviewed in this section.

Griffith Fracture Theory

When a crack is introduced in a stressed plate, two counteracting phenomena occur: elastic energy is released and surface energy is increased by the presence of the crack. If the former (which promotes growth) is larger than the latter (which impedes growth), crack propagation continues.

If an elliptical crack of length *a* is introduced into a plate of thickness δ),(Fig. 11.16) the total surface energy created is:

$$E_{surf} = 2a\delta\gamma_{surf} \tag{11.41}$$

where γ_{surf} is the energy per unit crack surface area. The elastic energy released by the crack is estimated [14] as:

$$E_{el} = \frac{\pi\sigma^2 a^2 \delta}{4E} \tag{11.42}$$

where σ is the applied stress, and *E* is the elastic modulus.

Thus the overall change in energy is

$$\Delta E_{crack} = -\frac{\pi\sigma^2 a^2 \delta}{4E} + 2a\delta\gamma_{surf} \tag{11.43}$$

Differentiating with respect to *a* and setting the result equal to zero, the equilibrium condition is:

$$\frac{\pi\sigma^2 a}{2E} = 2\gamma_{surf} \tag{11.44}$$

From which the stress for unstable crack propagation is:

$$\sigma = 2\sqrt{\frac{E\gamma_{surf}}{\pi a}} \tag{11.45}$$

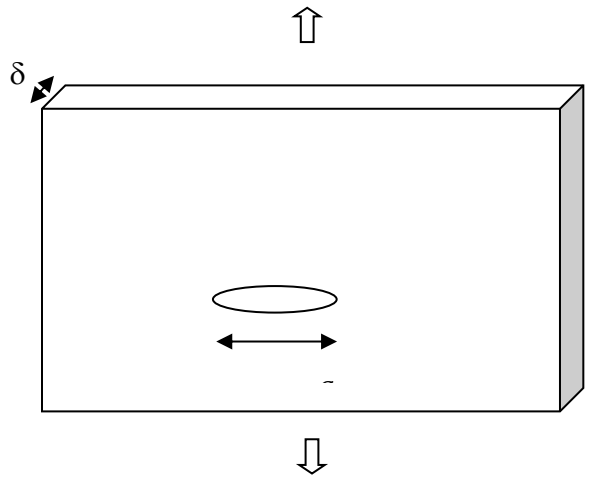

Fig. 11.16: an elliptical crack in a stressed plate

Eq. (11.45) can be rearranged as

$$(\sigma\sqrt{\pi a})_{crit} = \sqrt{2E\gamma_{surf}} = K_{IC} \tag{11.46}$$

The right-hand side of Eq(11.46) contains only material properties. The magnitude of this parameter that causes failure under a specific set of conditions is called the *fracture toughness* of the material K_{IC}. The fracture toughness is measured in the laboratory with carefully prepared cracks in test specimens

This condition for unstable crack propagation based on these two energetic processes was derived by Griffith in 1921. However, except in very brittle materials, this theory underpredicts measured values of K_{IC}. This is because in materials which exhibit some ductility it is necessary to induce plastic deformation prior to fracture. This occurs in a region ahead of the crack called the *plastic zone.* The Griffith derivation can be corrected for the creation of the plastic zone by

$$(\sigma\sqrt{\pi a})_{crit} = \sqrt{2E(\gamma_{surf} + \gamma_{pz})} = K_{IC} \tag{11.47}$$

where γ_{pz} is the energy per unit crack area to create a fracture surface that requires plastic work within the plastic zone at the crack tip. Equation (11.39) indicates that the higher the elastic modulus and the surface and (especially) the plastic work energies, the greater the fracture toughness.

The stress intensity factor is defined by[2]:

[2] The stress intensity factor is to fracture toughness as stress is to the yield stress.

$$K_I = Y\sigma\sqrt{a} \tag{11.48}$$

where Y is a constant usually having values between 1 and 2, depending on the geometry of the crack. The crack is assumed to be a "mode I" crack oriented normal to the applied stress σ. Formulas for Y for many different geometries are available [14].

If the maximum allowable crack length is substituted into Eq (11.48), the design stress σ *is* obtained if K_{IC} is known.

11.5.4. Subcritical Crack Growth

In an inert environment with $K_I < K_{IC}$, cracks are indefinitely stable in the absence of creep. However in an aggressive environment failure can occur by subcritical crack growth if

$$K_{IC} > K_I > K_{ISCC} \tag{11.41}$$

where K_{ISCC} is the stress intensity required for crack growth due to stress-corrosion cracking as discussed in Chapter 25. Alternatively, under cyclic loading with $K_I<K_{IC}$, there may be sufficient localized deformation occurring within the crack-tip plastic zone to advance the crack. If ΔK is the stress intensity range ($K_{max} - K_{min}$), then fatigue crack growth will occur if $\Delta K > \Delta K_{th}$, where ΔK_{th} is the threshold stress intensity factor for fatigue crack growth.

Problems

11.1 A metal rod of initial length l_0 and cross sectional area A_0 is tested uniaxially by fixing one end of the rod to a stationary point and loading the other with a spring of force constant K. The change in length of the rod, $l-l_0$, is related to the change in length of the spring, Δx, by:

$$\Delta x = \Delta x_Y - a(l-l_0)^2 + b(l-l_0)$$

where the first term on the right is the spring extension at the yield point of the rod and **a** and **b** are empirical constants.

(a) Express the true stress σ_x in terms of the true (logarithmic) strain ε_x and the parameters K, A_0, l_0, a, b, and Δx_Y. Do not assume a functional relation between these two variables(e.g., Eq(7.3)). Neglect elastic strain.

(b) Use the criterion for plastic instability to determine the true strain at the UTS.

11.2

The true stress-true strain curve in the work-hardening region can be written in dimensionless form:

$$\frac{\sigma - \sigma_Y}{\sigma_Y} = A\left(\varepsilon - \varepsilon_Y\right)^n$$

where the subscript Y denotes the yield point, A is a dimensionless constant, and n is the work-hardening coefficient. Define $X = (\sigma_{UTS} - \sigma_Y)/\sigma_Y$, where UTS denotes the ultimate tensile stress.

(a) What is the equation relating X to A and n?

(b) solve this equation for A = 23 and n = 0.7.

(c) show that X increases with n at constant A

11.3 For a particular metal, the true stress and the true strain obey the following plastic constitutive law: $\sigma_x = \sigma_Y \exp(\varepsilon_x - \varepsilon_Y)$. Prove that this material has no work-hardening region.

11.4

A closed cylindrical tube is pressurized to exceed yielding by 20%. The constitutive equation for the material of the tube in the plastic region is: $\sigma_x - \sigma_Y = C\varepsilon_x^n$ (elastic strain at the yield point is negligible).

(a) What are the stresses in the tube wall in terms of the uniaxial yield stress of the material?

(b) The plastic "strength" of the material is defined by: $S = (\sigma^* - \sigma_Y)/\varepsilon^*$, where σ^* and ε^* are the equivalent stress and strain, respectively. Determine S.

(c) What are the radial, azimuthal, and axial plastic strain components in the tube wall?

11.5

A spherical shell of radius R and wall thickness δ is pressurized internally to a pressure p.

(a) What stress components are nonzero and what are their values(use a force balance as in Sect. 5 for the pressurized cylinder)

(b) If the uniaxial yield stress is σ_Y, at what internal pressure will the shell yield?

11.6 The creep law of a particular steel is found in uniaxial tests to obey:

$$\dot{\varepsilon} = 161\sigma^{6.4} \exp(-3\times10^4 / T)$$

where the strain rate is in hr^{-1}, the stress is in MPa, and the temperature in Kelvin.

A component fabricated from this steel operates at 330°C. The principal normal stress components at a particular location are σ_x = 380 MPa, σ_y = 220 MPa and σ_z = 180 MPa. How long is required for the creep strain (in any direction) to reach 2%?

11.7 A weight of mass **m** is suspended from a closed thin-wall tube of radius **R** and wall thickness δ with internal pressure **p**. The yield strength of the tube material is σ_Y. Allowing for a 25% safety factor, what is the maximum gas pressure in the tube?

11.8 A tensile test specimen is initially of length l_0 and cross sectional area A_0. The specimen is subjected to varying loads P and the deformation Δl measured at each. The data are correlated by the empirical equation:

$$P = c + b\Delta l - a(\Delta l)^2$$

where a, b and c are positive constants.

(a) What are the "engineering" yield and ultimate stresses of this material?
(b) Show how the true stress-true strain curve can be deduced from the above equation.

Neglect elastic deformations and assume all deformation to be plastic.

11.9 When tested uniaxially at a particular temperature, the creep rupture behavior of a batch of metal tubing obeys the equation: $\sigma_x = C\left(t_R\right)^{-1/m}$, where C and m are material properties. This equation is Eq (7.7) of the notes with the temperature dependence included in the constant.

(a) When this tubing is sealed at both ends and pressurized at constant pressure p, what is the rupture time? The tube diameter is D and its wall thickness is δ.
(b) If the internal pressure varies linearly with time (p=kt), what is the time to failure?

11.10 A metal is tested in pure shear (σ_{xy} non zero but all the other stress components are zero). If the yield strength in a uniaxial tensile test is σ_{yuni}, what is the yield strength in the shear test $\sigma_{y\ shear}$?

11.11 A rod just fits between two rigid plates when its temperature is T_o. The rod is heated quickly and uniformly to a temperature T but the restraining plates do not move.

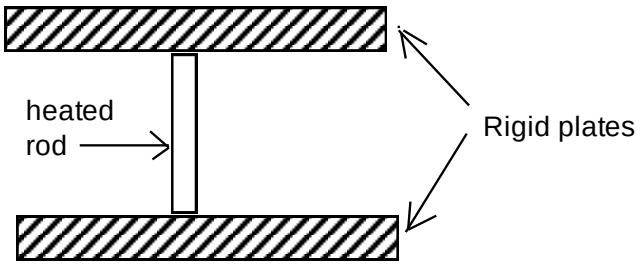

(a) What is the initial axial stress in the rod when the temperature reaches T? *Hint: Eq (5.14c) can be viewed as the total strain equal to the sum of the elastic and thermal strains, or* $\varepsilon_{tot} = \varepsilon_{el} + \varepsilon_{th}$.

(b) With time, the stress computed in part (a) is reduced because of creep (this is called *creep relaxation*). Since the thermal strain does not change with time, the total strain rate is the sum of the time rate of change of the elastic strain plus the creep strain rate, or $\dot{\varepsilon}_{tot} = \dot{\varepsilon}_{el} + \dot{\varepsilon}_{cr}$. At the final temperature T, the creep rate is $\dot{\varepsilon}_{cr} = B\sigma^n$, where the constant B includes the temperature effect. Derive the equation giving the variation of the axial stress in the rod with time.

Hint: in both parts (a) and (b) keep in mind that the total length of the rod remains constant.

References

[1] D. R. Olander, *Fundamental Aspects of Nuclear Reactor Fuel Elements*: ERDA, 1976.

[2] W. A. Backofen, *Deformation Processing*. Reading, MA: Addison-Wesley Publishing Co., 1972.

[3] T. H. Courtney, *Mechanical Behavior of Materials*. New York: McGraw-Hill, 1990.

[4] J. T. A. Roberts, *Structiral Materials for Nuclear Power Systems*: Plenum Press, 1981.

[5] A. S. Argon, *Strenghtening Mechanisms in Crystal Plasticity*: Oxfor University Press, 2008.

[6] L. M. Brown and R. K. Ham, "Dislocation-Particle Interactions," in *Streng\htening Methods in Crystals*, A. K. a. R. B. Nicholson, Ed. London: Applied Science Publishers Ltd., 1971.

[7] H. J. Frost and M. F. Ashby, *Deformation-Mechanism Maps, The Plasticity and Creep of Metals and Ceramics*, 1982.
[8] R. L. Klueh and D. R. Harries, *High Chromium Ferritic and Martensitic Steels for Nuclear Applications*. West Conshohocken, PA: ASTM, 2001.
[9] R. L. Klueh and A. T. Nelson, "Ferritic/martensitic steels for next-generation reactors," *Journal of Nuclear Materials*, vol. 371, pp. 37–52, 2007.
[10] M. F. Ashby, *Acta Metallurgica*, vol. 20, pp. 887, 1972.
[11] A. Considere, *Ann. Ponts et Chaussees*, vol. 9, pp. 574-775, 1885.
[12] A. Gurson, "Continuum theory of ductile rupture by void nucleation and growth : Part I – Yield criteria and flow rules for porous ductile media. ," *Journal of Engineering Materials and Technology*, vol. 99, pp. 2–15, 1977.
[13] D. Chae and D. A. Koss, "Damage accumulation and failure of HSLA-100 steel," *Materials Science and Engineering*, vol. A366, pp. 299-309, 2004.
[14] R. Hertzberg, *Deformation and Fracture Mechanics of Engineering Materials*, 3rd ed: Wiley, 1989.